Characterizing the Surface Roughness of Ejecta Fields Associated with Km-Scale Fresh Lunar Craters

G. W. Patterson(1), J. T. S. Cahill(1), D. B. J. Bussey(1), S. J. Lawrence(2), E. P. Turtle(1), M. S. Robinson(2), and the Mini-RF Team
(1) Planetary Exploration Group, Applied Physics Laboratory, 11100 Johns Hopkins Rd., Laurel, MD 20723, Wes.Patterson@jhuapl.edu (2) School of Earth and Space Exploration, Arizona State University, Tempe, AZ 85281

Introduction: Using the Mini-RF instrument and the Lunar Reconnaissance Orbiter Camera (LROC) Narrow Angle Camera (NAC) on NASA's Lunar Reconnaissance Orbiter (LRO), we have characterized the distribution of cm- to m-scale boulders associated with the ejecta of several km-scale fresh lunar craters. Understanding the size distribution of ejected material from impact craters can provide important information regarding the cratering process [1-4]. The typical method for determining distributions has relied on gathering statistics by counting impact-related features (*i.e.*, secondary craters [1,2] and boulders [3,4]) using visible image data on a small sample of craters. The goal of this research is to use such statistics for a small sample of km-scale fresh craters to characterize variations in surface roughness observed in radar data of the moon. This will eventually lead to a means of determining the size distribution of ejected material from km-scale impact craters without having to gather statistics by counting features, allowing a much larger sample size to be considered.

Background: Mini-RF is a hybrid-polarized, side-looking, synthetic aperture radar (SAR) on LRO. The instrument transmits at both S-band (12.6 cm) and X-band (4.2 cm) wavelengths and can operate in two modes: a baseline mode with a resolution of 150 m and a zoom mode with a resolution of 30 m [5,6]. Mini-RF measures returned signals in two orthogonal polarizations. These data allow for the calculation of Stokes parameters, which can be used to produce a variety of derived daughter products [7]. For this study, the relevant daughter product is Circular Polarization Ratio (CPR). CPR is defined as,

$$\mu_C = \frac{(S_1 - S_4)}{(S_1 + S_4)} \qquad (1)$$

where S_1 and S_4 represent the first and fourth Stokes parameters respectively, and it is an indicator of the roughness of a surface, as determined by the distribution of wavelength-scale and larger radar scatterers (*e.g.*, boulders). Young, fresh craters are distinctive in radar images obtained with the Mini-RF instrument (Fig. 1.) because of the surface roughness associated with their ejecta deposits [8].
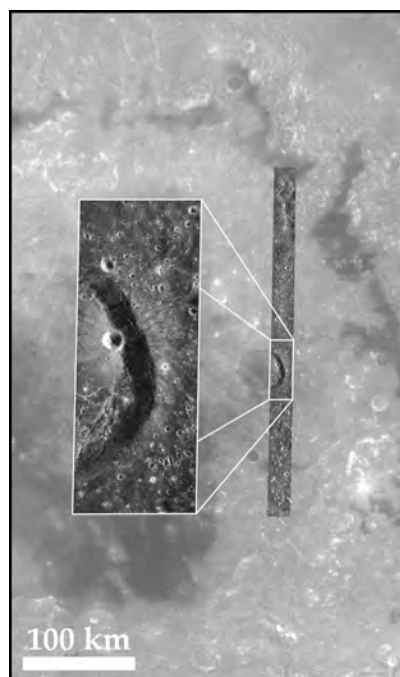

Fig. 1. S_1 image of Kopff crater within the Orientale basin extending from 21ºS to 11ºS latitude and centered at ~270.5ºE longitude. The data is overlain on Clementine UVVIS data at a resolution of 128 ppd. The inset (~30 m resolution) shows a fresh, unnamed crater within Kopff that has clearly defined ejecta deposits (Table 1).

The LROC NAC cameras on LRO are a pair of monochrome line scan imagers that acquire data at resolutions of up to 0.5 m [5,9]. In other words, these cameras observe the lunar surface at nearly the wavelength scale of the Mini-RF instrument. This means that we can use visible image data to characterize the distribution of radar scatterers that

are observed in Mini-RF CPR data and begin to understand how variations in such distributions affect CPR (*i.e.* ground-truth orbital radar data).

Methodology: We have identified several km-scale fresh lunar craters that have been observed by both Mini-RF and LROC NAC (Table 1). For each crater, we use total backscatter (S_1) (*e.g.*, Fig. 1.) and CPR information from Mini-RF data to characterize the extent of the ejecta field, as well the boundary between its continuous and discontinuous portions [8]. We use these boundaries to define areas that are representative of the different parts of the ejecta field, as well as the background terrain, and that have coincident LROC NAC coverage (*e.g.*, Fig. 2.). Boulders are then counted in the NAC images within the different areas to determine boulder distributions for each part of the crater. These distributions are compared to CPR information to relate surface roughnesses associated with different parts of the crater ejecta to the physical distribution of boulders observed.

Table 1.

Location	Diameter (km)	Description
17.2°S, 89.3°W	3	In crater Kopff[a]
27.9°S, 15.3°W	3	Hesiodus E
26.0°S, 26.1°W	2	Near crater Kies C
0.4°S, 32.7°E	4	Censorinus[b]
27.7°N, 11.8°E	2	Linne
36.5°N, 6.9°W	3	Kirch E
37.4°N, 8.1°W	3	Kirch G

[a]As seen in Fig. 1 and 2

[b]Statistics were previously gathered for this crater [4]

Summary: Using the Mini-RF and LROC NAC instruments aboard LRO, we have characterized the distribution of cm- to m-scale boulders associated with the ejecta of several km-scale fresh lunar craters. The results of this work will lead to a means of determining the size distribution of ejected material from km-scale impact craters without having to gather statistics through counting features. It will also lead, more generally, to a better understanding of the cratering process. The unnamed fresh crater on the floor of Kopff crater offers a specific example (Figs. 1 and 2). Here we observe that ejecta from the fresh crater has been deposited beyond the rim of Kopff. With the wall of Kopff acting as a topographic obstacle (Fig. 3), we can use statistics on the boulder population to better constrain models of ejecta emplacement.
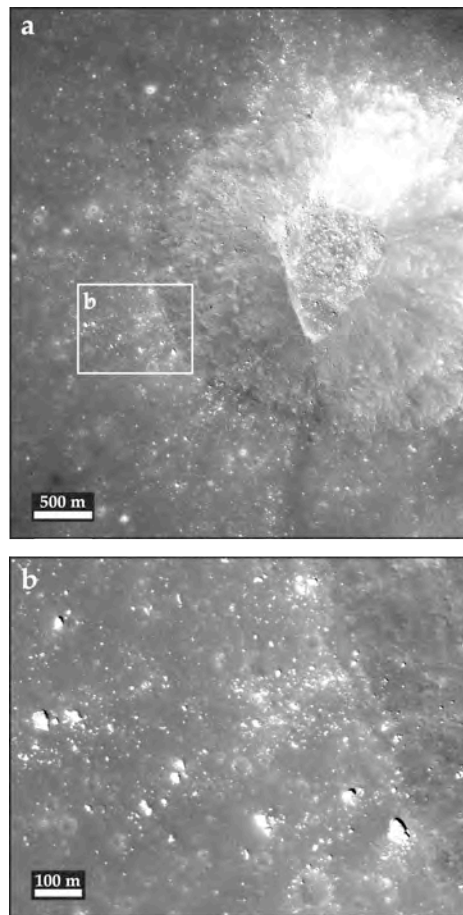

Fig. 2. (a) Portion of LROC NAC image (M122794259LE) acquired at an incidence angle of 26.6° showing the unnamed fresh crater seen in Fig. 1. The inset (b) shows boulders near the rim of the crater with sizes of 10s of meters down to the pixel scale of the image.
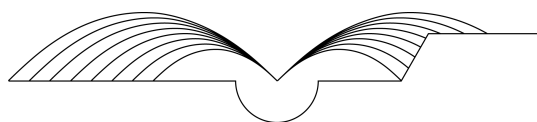

Fig. 3. Illustration of idealized trajectories for ejecta of varying velocity emplaced during an impact near the wall of the larger crater Kopff. Here only ejecta fragments with some minimum velocity could be emplaced beyond the wall of the crater.

References: [1] Vickery (1986), *Icarus*, 67, 224-236; [2] Vickery (1987), *GRL*, 14, 726-729; [3] Bart and Melosh (2007), *GRL*, 34, doi:10.1029/2007GL029306; [4] Bart and Melosh (2010), *Icarus*, 209, 337-357; [5] Chin et al. (2007), *Space Sci. Rev.,* doi:10.1007/s11214-007-9153-y; [6] Nozette et al., (2007), *Space Sci. Rev.*, 150, doi: 10.1007/s11214-009-9607-5; [7] Raney (2006), *IEEE Geosci. Rem. Sens. Lett., 3*, 317; [8] Patterson et al. (2010), *LPSC XXXXI*, #2316; [9] Robinson et al. (2007), *Space Sci. Rev.*, 150, doi: 10.1007/s11214-010-9634-2.